VOLUME 36 NUMBER 3
MARCH 2018

ISSN: 1002-0721
CODEN JREAE 6

Journal of Rare Earths

ELSEVIER

Project for Enhancing International Impact of China STM Journals

万方数据

CONTENTS

万方数据

JOURNAL OF RARE EARTHS
Vol. 36 No. 3 (March 2018)

CONTENTS

SPECTROSCOPY, LUMINESCENCE AND PHOSPHORS

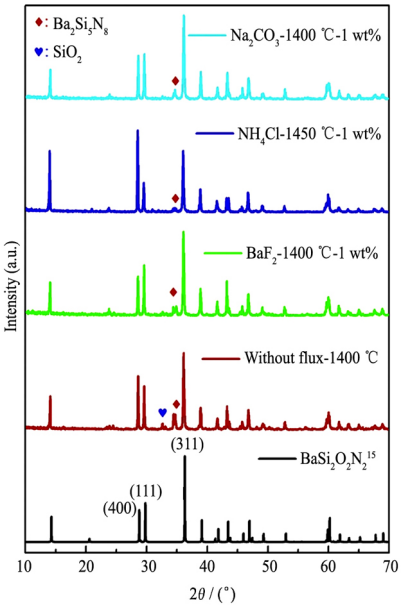

XRD patterns of the $BaSi_2O_2N_2:Eu^{2+}$ phosphor sintered at various temperatures without flux and with 1 wt% flux

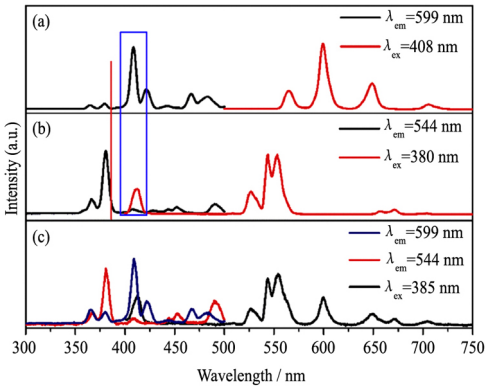

PLE and PL spectra of $Bi_{0.99}Sm_{0.01}OCl$ (a), $Bi_{0.99}Er_{0.01}OCl$ (b) and $Bi_{0.98}Er_{0.01}Sm_{0.01}OCl$ (c) phosphors

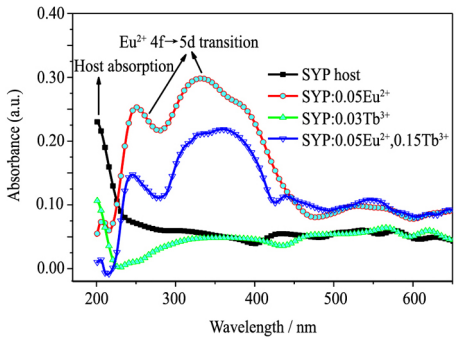

Eu^{2+}, Tb^{3+} co-doped $Sr_3Y(PO_4)_3$ phosphors were synthesized for the first time. Energy band gap of $Sr_3Y(PO_4)_3$ host material was significantly affected by doping with rare earths. Emission intensity of Tb^{3+} can be enhanced by co-doping with Eu^{2+}

万方数据

243 Luminescence properties of Pr^{3+} and Bi^{3+} co-doped $NaCaTiNbO_6$ phosphor for red-LEDs

Di Xu, Panlong Yu, Lianhua Tian

J. Rare Earths, (36) 2018: 243-247

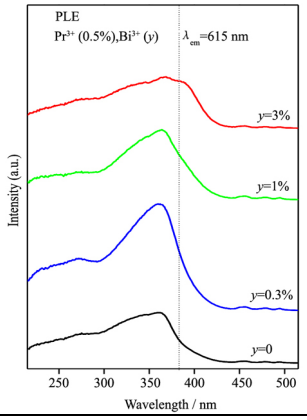

Excitation spectra of $NaCaTiNbO_6:Pr^{3+}$ with different Pr^{3+} concentrations

248 Combustion synthesis of YAG:Ce phosphors via the thermite reaction of aluminum

Junpei Ohyama, Chunyu Zhu, Genki Saito, Miki Haga, Takahiro Nomura, Norihito Sakaguchi, Tomohiro Akiyama

J. Rare Earths, (36) 2018: 248-256

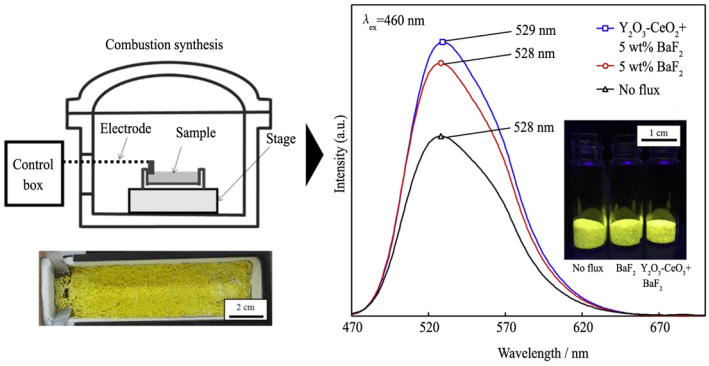

Schematic diagram of the experimental apparatus for combustion synthesis and emission spectra for the combustion-synthesized products under different conditions: no flux, 5 wt% BaF_2, and Y_2O_3-CeO_2 + 5 wt% BaF_2. The inset shows a photograph of the synthesized powders

RARE EARTH CATALYSIS

257 Effect of active oxygen on the performance of Pt/CeO_2 catalysts for CO oxidation

Anbin Zhou, Jun Wang, Hui Wang, Hang Li, Jianqiang Wang, Meiqing Shen

J. Rare Earths, (36) 2018: 257-264

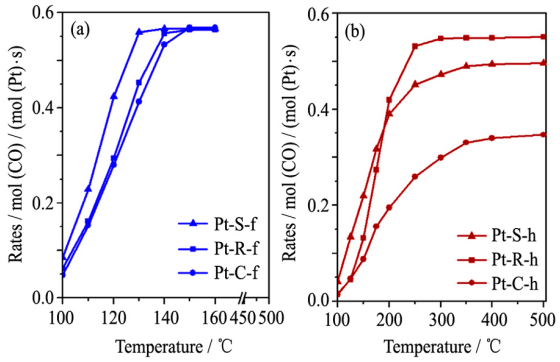

The more active oxygen on CeO_2 contributes to enhancing the Pt-CeO_2 interaction, which effectively increases the CO oxidation activity. The metallic Pt^0 is active in the low- temperature CO oxidation, while the oxidized $Pt^{\delta+}$ contributes to the activity at high temperature

265 Effect of coating modification of cordierite carrier on catalytic performance of supported $NiMnO_3$ catalysts for VOCs ombustion

Lei Deng, Chao Huang, Jiawei Kan, Bing Li, Yingwen Chen, Shemin Zhu, Shubao Shen

J. Rare Earths, (36) 2018: 265-272

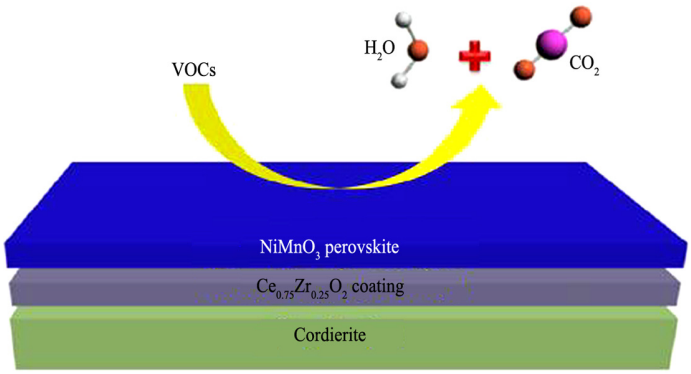

The $Ce_{0.75}Zr_{0.25}O_2$ coating can promote more lattice distortion and defects and smaller crystal size, which improves oxygen transfer capability and dispersion of active component

万方数据

273 Structural properties and catalytic performance of the La–Cu–Zn mixed oxides for CO_2 hydrogenation to methanol

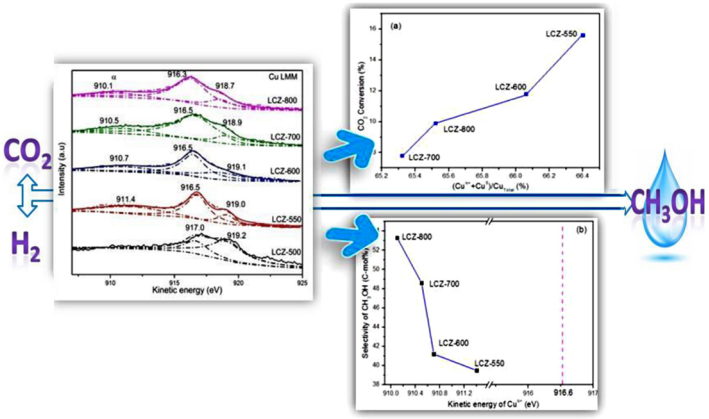

Haijuan Zhan, Zhiqiang Wu, Ning Zhao, Wanyi Liu, Wei Wei

La-Cu-Zn-O mixed oxide catalysts are synthesized and tested
The La_2CuO_4 perovskite forms at high temperature with special copper species.
Catalysts with La_2CuO_4 perovskite structure show higher methanol selectivity.
Both Cu^+ and Cu^0 are important active sites in perovskite for the reaction

J. Rare Earths, (36) 2018: 273-280

MAGNETISM AND MAGNETIC MATERIALS

281 Effect of niobium substitution on microstructures and thermal stability of $TbCu_7$-type Sm–Fe–N magnets

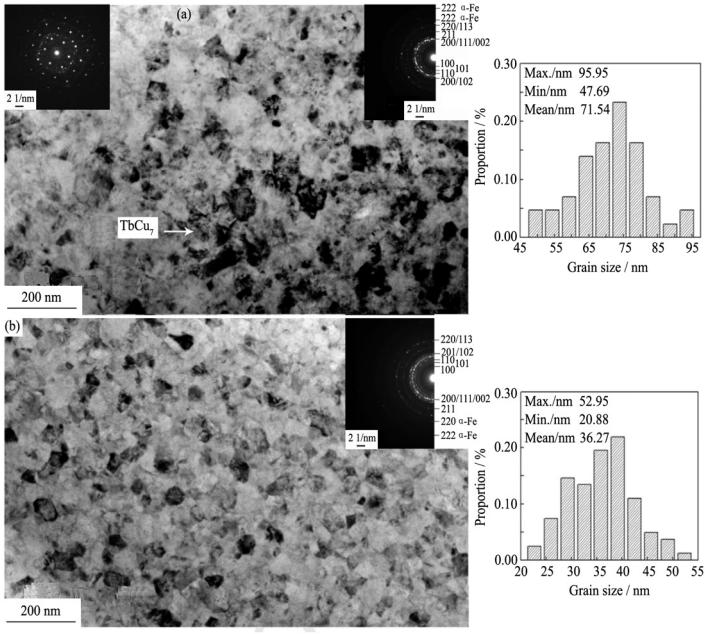

Guiyong Wu, Hongwei Li, Dunbo Yu, Kuoshe Li, Wenlong Yan, Chao Yuan, Liang Sun, Yang Luo, Kun Zhang

TEM micrographs and SAED patterns (inset) of as-annealed NB0 ribbons (a) and NB12 ribbons (b)

J. Rare Earths, (36) 2018: 281-286

ADVANCED RARE EARTH MATERIALS

287 Effect of calcination temperature on B-site vacancy content of $La_{0.75}Sr_{0.25}Mn_{0.92}\Delta_{0.08}O_{3-\delta}$ perovskite

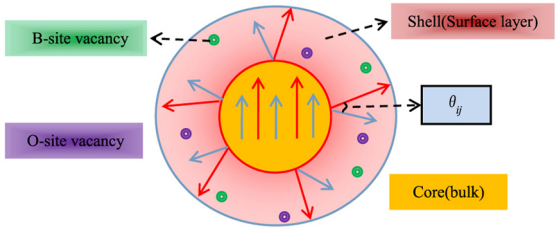

Denghui Ji, Shuling Wang, Xingze Ge, Xinju Xiao, Liwei Wang, Zhiwei Zeng, Congmin Zhang

Schematic diagrams (two dimensional) of the evolution of the magnetic configuration with particle size. Red or blue arrows represent the spins orientation of Mn^{3+} or Mn^{4+} cations, green or purple concentric circles represent the B-site or O-site vacancy. The magnetic moment angle θ_{ij} between Mn^{3+} cations and Mn^{4+} cations on the surface

J. Rare Earths, (36) 2018: 287-297

万方数据

298 Self-polymerization and co-polymerization kinetics of gadolinium methacrylate

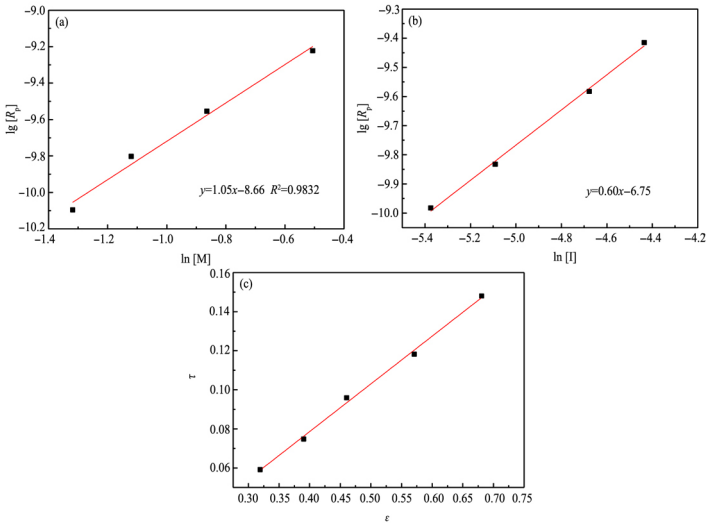

Chunhong Wang, Shuai Wang, Yujuan Zhang, Zhifeng Wang, Junliang Liu, Ming Zhang

The polymerization rate of $Gd(MAA)_3$: $R_p = K[M]^{1.05}[I]^{0.60}$. The reactivity ratios of MMA and $Gd(MAA)_3$: r_1(MMA)=0.225, r_2($Gd(MAA)_3$)=1.340

J. Rare Earths, (36) 2018: 298-303

CHEMISTRY AND HYDROMETALLURGY

304 Extraction and separation of heavy rare earths from chloride medium by α-aminophosphonic acid HEHAPP

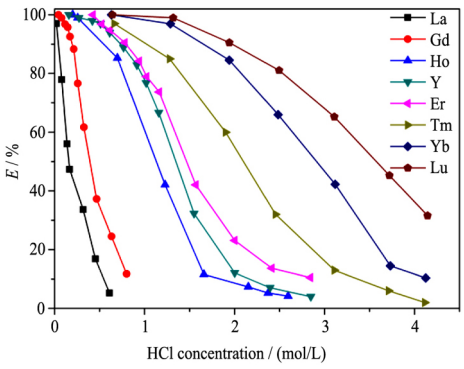

Shengting Kuang, Zhifeng Zhang, Yanling Li, Haiqin Wei, Wuping Liao

The aminophosphonic acid extractant HEHAPP exhibits relatively higher extraction ability and stronger separation ability for heavy rare earths than P507 and Cyanex 272

J. Rare Earths, (36) 2018: 304-310

311 Removal of impurities from scandium chloride solution using 732-type resin

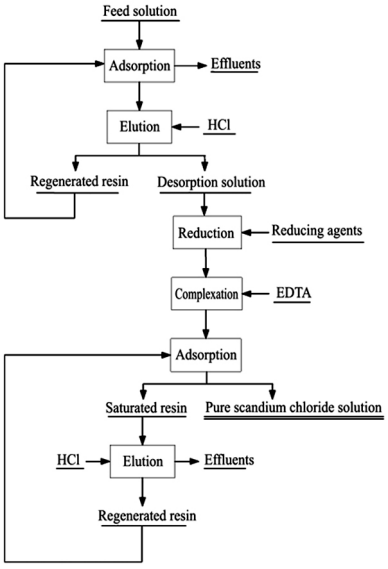

Guotao Zhou, Qinggang Li, Pan Sun, Wenjuan Guan, Guiqing Zhang, Zuoying Cao, Li Zeng

A new two-step ion exchange process for removing impurities such as Al, Fe(Ⅲ), Ca, Zr, Ti and Si from scandium chloride solution has been proposed in this paper. By using this new process, the removal rate of Fe(Ⅲ), Ti, Al, Ca, Zr and Si reached to 95.5%, 99.8%, 100%, 98.2%, 98.6% and 100%, respectively

J. Rare Earths, (36) 2018: 311-316

万方数据

317 Solvent extraction and separation of light rare earth elements (La, Pr and Nd) in the presence of lactic acid as a complexing agent by Cyanex 272 in kerosene and the effect of citric acid, acetic acid and Titriplex III as auxiliary agents

Eslam Kashi, Razieh Habibpour, Hesamoddin Gorzin, Armin Maleki

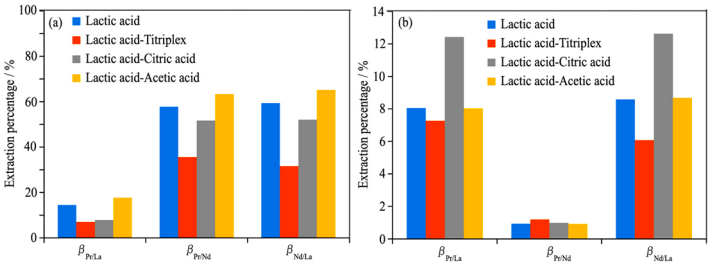

Effect of citric acid, acetic acid and Titriplex III in Cyanex272-HLac-HCl system

(a) Extraction percentage; (b) Separation factor

J. Rare Earths, (36) 2018: 317-323

METALLOGRAPHY AND PYROMETALLURGY

324 Cathodic reduction process of Al–Cu–Y alloy in fluoride-oxide eutectic system via molten salt electrolysis

Xu Wang, Chunfa Liao, Yunfen Jiao, Hao Tang

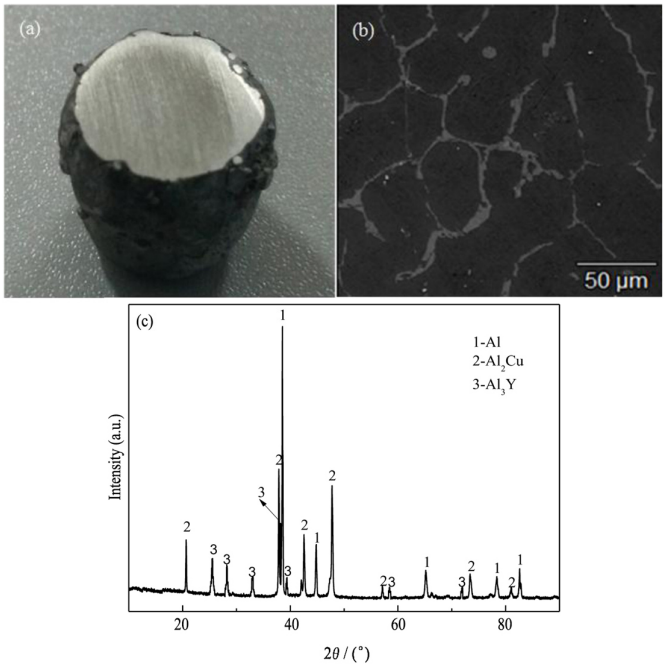

Digital image of electrolysis alloy samples showing good metallic luster (a); SEM image (b) and XRD pattern (c) of the Al-Cu-Y alloy sample

J. Rare Earths, (36) 2018: 324-330

RARE EARTH APPLICATIONS

331 Bioaccumulation, subcellular distribution and chemical forms of yttrium in rice seedling

Shengnan Zheng, Caiyun Zhang, Kailun Shi, Jinxiao Wang, Guanjun Sun, Qiaochu Hu, Fengyun Zhao, Xue Wang

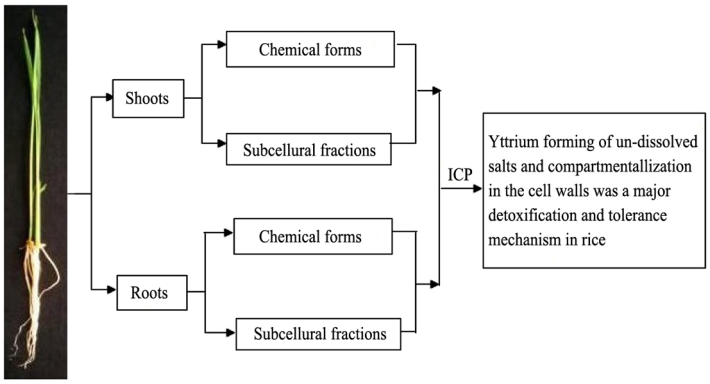

Intracellular localization and chemical forms of Y in rice

J. Rare Earths, (36) 2018: 331-336

万方数据